DOMINICAN UNIVERSITY of CALIFORNIA

Dominican Scholar

Collected Faculty and Staff Scholarship | Faculty and Staff Scholarship

2000

Photoabsorption Spectra of Argon Cation Clusters: Monte Carlo Simulations Using Many-body Polarization

Jose A. Gascon
Department of Chemistry, Louisiana State University, Baton Rouge

Randall W. Hall
Department of Chemistry and Department of Physics, Louisiana State University, Baton Rouge, randall.hall@dominican.edu

Survey: Let us know how this paper benefits you.
Follow this and additional works at: https://scholar.dominican.edu/all-faculty
 Part of the Physical Chemistry Commons

Recommended Citation
Gascon, Jose A. and Hall, Randall W., "Photoabsorption Spectra of Argon Cation Clusters: Monte Carlo Simulations Using Many-body Polarization" (2000). *Collected Faculty and Staff Scholarship*. 199.
https://scholar.dominican.edu/all-faculty/199

DOI
http://dx.doi.org/https://doi.org/10.1063/1.1312825

This Article is brought to you for free and open access by the Faculty and Staff Scholarship at Dominican Scholar. It has been accepted for inclusion in Collected Faculty and Staff Scholarship by an authorized administrator of Dominican Scholar. For more information, please contact michael.pujals@dominican.edu.

Photoabsorption spectra of argon cation clusters: Monte Carlo simulations using many-body polarization

Jose A. Gascon
Department of Chemistry, Louisiana State University, Baton Rouge, Louisiana 70803

Randall W. Hall[a)]
Department of Chemistry and Department of Physics, Louisiana State University, Baton Rouge, Louisiana 70803

(Received 9 May 2000; accepted 4 August 2000)

A simple, semiempirical model that includes many-body polarization is used to study the ground and excited state properties of Ar_N^+ clusters ($N=3-23$) at 80 K. For purposes of comparison, a model that does not include many-body polarization is used to study clusters with $N=3-27$. Monte Carlo simulations are used to calculate the average properties of these clusters. The model is similar to one previously used to study argon cation clusters without many-body polarization. The photoabsorption spectrum is in good agreement with experiment; in particular, the photoabsorption spectra for cluster sizes 4–10 do not show the blueshift that is seen with models that do not include many-body polarization. © *2000 American Institute of Physics.* [S0021-9606(00)30141-6]

I. INTRODUCTION

The electronic and geometric structures of argon cation clusters have received both experimental[1–12] and theoretical[13–24] interest over the past few years. The focus has been to understand the extent of delocalization of the positive charge (hole) and the evolution of the photoabsorption cross section as a function of cluster size. Previous theoretical studies using a tight-binding model[21] and a diatomics-within-molecules (DIM) approach[13,14] have predicted a relatively large blueshift in the photoabsorption spectrum between three and seven atoms which is not seen in experiment. Neither model included many-body polarization (MBP), which may be important for polarizable atoms such as argon. Recent DIM calculations have included polarization effects through a three-body interaction in the simulation of photoabsorption spectra. Grigorov and Spiegelmann[22] reported calculation for $N=3$, 4, 8, 13, and 19 at finite temperature while Doltsinis *et al.*[23] reported simulations at 0 K for $N=3$. However, there has yet to be a study that includes polarization for all clusters from $N=3-23$.

In this work, we use a semiempirical tight-binding Hamiltonian that includes many-body polarization to study Ar_N^+ clusters at finite temperature. The form of the Hamiltonian is similar to the one previously used[21] and includes simple, physically reasonable terms, which are either fixed using known properties such as the polarizability of neutral Ar or by fitting to the spectral and structural properties of Ar_2, Ar_2^+, Ar_3, and Ar_3^+. We calculate the thermally averaged electronic photoabsorption spectrum and charge distribution for clusters with $N=3-23$ at a temperature of 80 K. We also calculate the photoabsorption spectra without using MBP for $N=3-27$. Finally, we determine the minimum energy geometries at 0 K using MBP to investigate the most stable clusters in the range of $N=3-26$.

II. MODEL HAMILTONIAN

Our Hamiltonian uses three basis functions per atom since the charge is in a *p*-type orbital and has the following form:

$$H=H_{\mathrm{Ar-Ar}}+H_{\mathrm{Ar^+-Ar}}+E_{\mathrm{MBP}}+t, \tag{1}$$

where the first three terms give the diagonal elements and the last term gives the hopping matrix elements. $H_{\mathrm{Ar-Ar}}$ is the short range repulsion interaction between neutral Ar atoms and is given by

$$H_{\mathrm{Ar-Ar}}=\sum_{k,v}|k,v\rangle\left(\sum_{\substack{i,j\neq k\\ j>i}}Ae^{-Br_{ij}}\right)\langle k,v|, \tag{2}$$

where $|k,v\rangle$ represents a *p*-type orbital on atom k with orientation v (representing the $\hat{x}$, $\hat{y}$, or $\hat{z}$ directions), and i and j label atoms. $H_{\mathrm{Ar^+-Ar}}$ is the short range repulsion between the atom with the charge and the neutral atoms:

$$H_{\mathrm{Ar^+-Ar}}=\sum_{k,v}\sum_{i\neq k}|k,v\rangle(A^+e^{-B^+r_{ki}})\langle k,v|. \tag{3}$$

E_{MBP} is the polarization energy of a system of N atoms in the presence of a charge:

$$E_{\mathrm{MBP}}=\sum_{k,v}|k,v\rangle E_{\mathrm{MBP}}(k)\langle k,v|, \tag{4}$$

where the explicit form for $E_{\mathrm{MBP}}(k)$, assuming a Drude oscillator model for the fluctuating dipoles on the argon atoms, is

$$E_{\mathrm{MBP}}(k)=\sum_{i=1}^{3N}\frac{1}{2}\left(\sqrt{\lambda_i(k)}-\frac{X_i^2(k)}{\lambda_i(k)}-\omega_i\right), \tag{5}$$

a)Electronic mail: rhall@lsu.edu

 © 2000 American Institute of Physics

Downloaded 26 Apr 2004 to 130.132.248.10. Redistribution subject to AIP license or copyright, see http://jcp.aip.org/jcp/copyright.jsp

TABLE I. Parameters of the model Hamiltonian; all numbers are in atomic units.

MBP parameters										
A	B	A^+	B^+	a	b	c	α	α^+	ω	ω^+
180.845	1.8361	1514.41	2.1936	1.5949	1.9579	0.6495	11.09	6.5	1.1649	2.2045
Without MBP										
A	B	A^+	B^+	a	b	c	C_6	C_6^+	σ^a	
172.520	1.8314	2164.39	2.2823	1.9159	1.9782	0.6172	95.310	107.448	5.4341	

[a]See Ref. 21 for its definition.

X_i is the shift in the normal mode minimum due to the field from the charge on atom k, λ_i is the normal mode frequency in the absence of the electric field, and ω_i is the unperturbed atomic normal mode frequency. Equation (5) is derived in Sec. III. We note that within the Drude oscillator model Eq. 5 is the exact solution to an N-body problem.

The form of the hopping term is estimated from its form for a two-atom cluster: $\langle \Psi_i | T+V_i+V_j | \Psi_j \rangle$, where Ψ_i and Ψ_j are the wave functions of the hole being localized in atoms i and j, respectively, T is the kinetic energy, and V_i is the potential energy of the hole interacting with atom i. Assuming Slater $2p$-type orbitals we obtain

$$t_{ij}^{\gamma\eta} = -ae^{-br_{ij}}\left[\mathbf{e}_\gamma\cdot\mathbf{e}_\eta(1+br_{ij}+\tfrac{1}{3}b^2r_{ij}^2) - \frac{b^2}{3}(\mathbf{e}_\gamma\cdot\mathbf{r}_{ij})(\mathbf{e}_\eta\cdot\mathbf{r}_{ij})(1+br_{ij})\right] - cs_{ij}^{\gamma\eta}, \tag{6}$$

where $s_{ij}^{\gamma\eta}$ is the overlap matrix

$$s_{ij}^{\gamma\eta} = e^{-br_{ij}}\left[\mathbf{e}_\gamma\cdot\mathbf{e}_\eta(1+br_{ij}+\tfrac{2}{5}b^2r_{ij}^2+\tfrac{1}{15}b^3r_{ij}^3) - \frac{b^2}{5}(\mathbf{e}_\gamma\cdot\mathbf{r}_{ij})(\mathbf{e}_\eta\cdot\mathbf{r}_{ij})(1+br_{ij}+\tfrac{1}{3}b^2r_{ij}^2)\right]. \tag{7}$$

The parameters of the model are determined from known experimental values or by fitting the Ar_N and Ar_N^+ ground and excited state properties for $N=1-3$. This is distinct from our previous work,[21] in which only monomer and dimer properties were used to determine parameters. The polarizability and C_6 coefficient for Ar are taken from the literature.[25,26] To determine ω_{Ar} and ω_{Ar^+}, we use the relation given by Cao and Berne[27] for a Drude oscillator model of the atoms, viz. $C_6=\frac{3}{4}\omega\alpha^2$ for a pure system and $C_6'=\frac{3}{4}[2\omega_1\omega_2/(\omega_1+\omega_2)]\alpha_1\alpha_2$ for a mixture, where the α's are polarizabilities and the ω's are frequencies of the Drude oscillators. ω_{Ar} is determined with knowledge of C_6 and α_{Ar}. We consider Ar_2^+ as a mixture of Ar and Ar^+ and thus we need the frequency and polarizability of Ar. We obtain α_{Ar^+} by using previously performed *ab initio* calculations of the polarizabilities of Ar and Ar^+ and scaling the literature value of α_{Ar} by the ratio of the polarizabilities determined in the *ab initio* calculations. We assume that the ratio of ω's is the same as the ratio of ionization potentials of Ar and Ar^+, which was then used to estimate ω_{Ar^+} from ω_{Ar}. A, B, A^+, B^+, a, b, and c were determined by fitting to the bond length, dissociation, and excitation energies for Ar_N and Ar_N^+ with $N=2-3$. The model Hamiltonian for the case without MBP is described in our previous work[21] except for a modification in the off diagonal terms that we present in this work. The parameters for the current models are shown in Table I. The procedure for calculating the photoabsorption spectrum is as follows: if $|a\rangle=\Sigma_{i,\gamma}c_{ai\gamma}|i\gamma\rangle$ is the eigenvector of the ath state (assumed real and p-type functions), then the transition dipole between state 0 and a for a given configuration is given by

$$\mu_{0a}^{\xi} = \langle 0|r^{\xi}|a\rangle = \sum_{i,j,\gamma,\eta} c_{0i\gamma}c_{aj\eta}s_{ij}^{\gamma\eta}\times\left(\frac{r_i^{\xi}+r_j^{\xi}}{2}\right),$$

where $s_{ij}^{\gamma\eta}$ is the overlap matrix defined above and $\xi=x$, y, or z. Finally, the photoabsorption intensity is reported as a function of the wavelength:

$$I(\lambda) = s_0\hbar\frac{\lambda^2}{\Delta\lambda}\frac{1}{N_c}\sum_l\sum_a\frac{1}{\lambda_{0a}}|\boldsymbol{\mu}_{0a}(l)|^2 \times\Theta\left(\lambda_{0a}-\lambda+\frac{\Delta\lambda}{2}\right)\Theta\left(\lambda+\frac{\Delta\lambda}{2}-\lambda_{0a}\right),$$

where $\Delta\lambda$ is the resolution in the wavelength, Θ is the Heaviside step function, N_c the number of sampled configurations, and

$$s_0=\frac{1}{4\pi\epsilon_0}\frac{4\pi^2}{3c\hbar^2}.$$

III. MANY-BODY POLARIZATION

We now discuss the inclusion of many-body polarization. We only include many-body polarization in the diagonal matrix elements of the Hamiltonian, which is consistent with our previous work. We follow the work by Cao and Berne[27] and treat the polarizability of the atoms using a Drude model. Since the diagonal matrix elements correspond to the charge being localized on one atom, we can write the Hamiltonian for the Drude oscillators as

$$H=\sum_{i=1}^{N}\left(\frac{\dot{\boldsymbol{\mu}}_i^2}{2\alpha_i\omega_i^2}+\frac{\boldsymbol{\mu}_i^2}{2\alpha_i}\right)-\frac{1}{2}\sum_{i=1}^{N}\sum_{j\neq 1}^{N}\boldsymbol{\mu}_i\cdot T_{ij}\cdot\boldsymbol{\mu}_j - \sum_{\substack{i=1\\ i\neq k}}^{N}\boldsymbol{\mu}_i\cdot\mathbf{E}_i(k),$$

Downloaded 26 Apr 2004 to 130.132.248.10. Redistribution subject to AIP license or copyright, see http://jcp.aip.org/jcp/copyright.jsp

where the charge is localized on atom k, $\boldsymbol{\mu}_i$ is the dipole moment of atom i, T_{ij} is the dipole–dipole tensor whose matrix elements are given by

$$T_{ij}^{\mu\nu}=\frac{3\mathbf{r}_{ij}^{\mu}\mathbf{r}_{ij}^{\nu}-\delta^{\mu\nu}\mathbf{r}_{ij}^{2}}{\mathbf{r}_{ij}^{5}},$$

α_i is the polarizability of atom i, ω_i is the frequency of oscillator i, and $\mathbf{E}_i(k)$ is the electric field at atom i due to a charge on atom k. Making the substitution $\boldsymbol{\mu}_i=\sqrt{\alpha_i}\omega_i\mathbf{z}_i$, the Hamiltonian becomes

$$\sum_{i=1}^{N}\frac{\dot{\mathbf{z}}_i^2}{2}+\frac{1}{2}\sum_{i=1}^{N}\sum_{j=1}^{N}\mathbf{z}_i\cdot M_{ij}\cdot\mathbf{z}_j-\sum_{\substack{i=1\\ i\neq k}}^{N}\sqrt{\alpha_i}\omega_i\mathbf{z}_i\cdot\mathbf{E}_i(k),$$

where the matrix M_{ij} is defined by

$$M_{ij}\equiv\omega_i^2\delta_{ij}-\sqrt{\alpha_i\alpha_j}\omega_i\omega_j T_{ij}(1-\delta_{ij}).$$

Let us define

$$\mathbf{Z}=(\mathbf{z}_1,\ldots,\mathbf{z}_k,\ldots,\mathbf{z}_N),\quad \mathbf{Q}=(\mathbf{q}_1,\ldots,\mathbf{q}_k,\ldots,\mathbf{q}_N),$$

$$\mathbf{Y}=[\sqrt{\alpha_1}\omega_1\mathbf{E}_1(k),\ldots,\mathbf{0},\ldots,\sqrt{\alpha_N}\omega_N\mathbf{E}_N(k)].$$

If $\mathbf{M}$ is diagonalized via $\mathbf{Z}=\mathbf{U}\cdot\mathbf{Q}$, where $\mathbf{U}$ is a unitary transformation, the Hamiltonian becomes

$$\tfrac{1}{2}\dot{\mathbf{Q}}^2+\tfrac{1}{2}\mathbf{Q}\cdot\mathbf{M}'\cdot\mathbf{Q}-\mathbf{Y}\cdot\mathbf{U}\cdot\mathbf{Q},$$

where $\mathbf{M}'$ is a diagonal matrix whose elements are the eigenvalues of $\mathbf{M}$. If we define $\mathbf{X}=\mathbf{Y}\cdot\mathbf{U}$, then the Hamiltonian becomes

$$\frac{1}{2}\left[\sum_{i=1}^{3N}\dot{Q}_i^2+\sum_{i=1}^{3N}\lambda_i\left(Q_i-\frac{X_i}{\lambda_i}\right)^2-\frac{X_i^2}{\lambda_i}\right],$$

where λ_i are the eigenvalues of $\mathbf{M}$. This is the Hamiltonian of $3N$ independent harmonic oscillators with a ground state energy

$$\sum_{i=1}^{3N}\frac{1}{2}\left[\sqrt{\lambda_i}-\frac{X_i^2}{\lambda_i}\right].$$

To finally obtain the interaction energy we need to subtract the energy of $3N$ independent Drude oscillators:

$$E_{\mathrm{MBP}}=\sum_{i=1}^{3N}\frac{1}{2}\left(\sqrt{\lambda_i}-\frac{X_i^2}{\lambda_i}-\omega_i\right).$$

IV. RESULTS

All calculations are performed at a temperature of 80 K. The initial configuration is obtained by combining a simulated annealing with a conjugate gradient minimization for the model without MBP. The starting geometry for this procedure is generated by randomly placing the Nth atom around the cluster of $N-1$ atoms. The minimized geometry is then used as the initial configuration in the finite temperature calculations for both models, with and without MBP. A Monte Carlo (MC) simulation of 120 000 steps for small clusters (3–13) and 80 000 (14–23) for large clusters is performed to calculate the average properties.

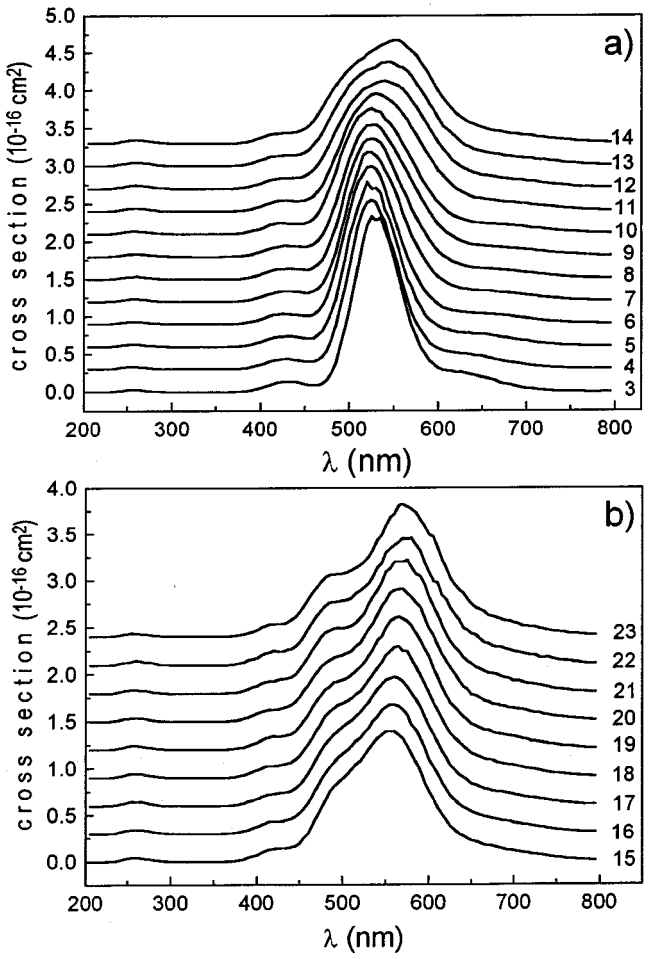

FIG. 1. Calculated photoabsorption cross section. The curves are vertically shifted 0.3×10^{-16} cm^2 from each other. (a) From $N=3$ to 14. (b) From $N=15$ to 21.

A. Photoabsorption spectrum

In Fig. 1 we show the photoabsorption spectra as a function of the cluster size. Between $N=3-14$ [Fig. 1(a)] we observe three peaks in the spectra. The first peak is located at about 260 nm. It was seen experimentally by Johnson and co-worker.[8] Although this region is commonly referred to as a dimer remnant, the average charge for the ground state is distributed in a trimer core for $N>3$.[21] In terms of Ar_3^+ states, such energies correspond to states with nodes between the central atom and its two neighbors ($2^2\Sigma_u^+$).[28] A second peak is located at about 425 nm and is characterized by the symmetry $2^2\Pi_u$. Although these transitions ($1^2\Sigma_u^+ \rightarrow 2^2\Sigma_u^+, 2^2\Pi_u$) are forbidden for a linear symmetric trimer, they emerge due to instantaneous vibrational symmetry breaking. A third and main peak is located at about 520 nm and is associated with the Ar_3^+ transition $1^2\Sigma_u^+\rightarrow 1^2\Sigma_g^+$. At $N=10$ this main peak redshifts to a final location around 570 nm for $N=23$. From $N=15$ [Fig. 1(b)] a high energy shoulder emerges and finally resolves at $N=21$. This same trend occurs for the model without MBP for $N>14$. However, without MBP, for $N\leqslant 14$ the spectra continue blueshifting and abruptly redshift at $N=14$. For comparison with previous experimental and theoretical work, we calculate the

Downloaded 26 Apr 2004 to 130.132.248.10. Redistribution subject to AIP license or copyright, see http://jcp.aip.org/jcp/copyright.jsp

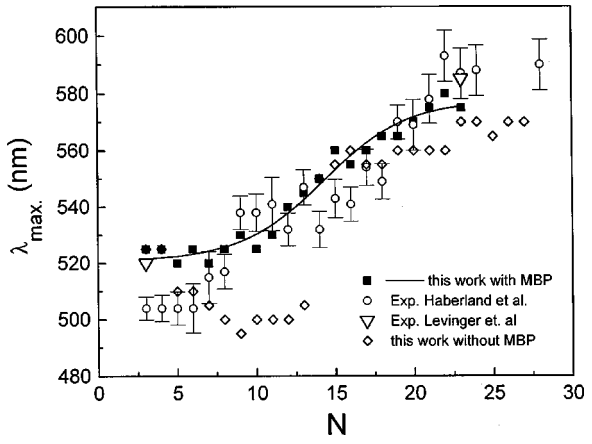

FIG. 2. Average wavelength at the maximum peak as a function of cluster size. (■) Our results using many-body polarization. The solid line through the MBP points is only drawn to guide the eye. (◇) Our results without using many-body polarization. (○) Experiment from Ref. 9. (▽) Experiment from Ref. 10.

wavelength (λ_{max}) at the maximum of the photoabsorption spectrum with a resolution $\Delta\lambda = 5$ nm. The results are shown in Fig. 2, along with results without using MBP and experiment. A particular feature of the experimental spectra is the absence of a blueshift for small clusters. Levinger *et al.*[10] (shown by open triangles in Fig. 2) reported spectra of Ar_N^+ for sizes $N = 3-23$. They claim that clusters between $N = 4$ and 15 present a similar spectrum to that of Ar_3^+ with a peak near 520 nm. Our spectrum for Ar_3^+ presents its peak at 525 nm and it is narrower than the spectrum obtained by Levinger *et al.* by about 30%. Consequently, the peak is higher by about 35%. We are not including spin–orbit coupling and zero-point energy effects which could lead to better agreement in terms of the width and height of the peak. Haberland *et al.*[9] (shown by open circles in Fig. 2) reported no blueshift from $N = 3-6$ after which they saw mainly a redshift and finally a constant value for $N > 20$. Our results using MBP agree very well with this trend. We find a maximum blueshift of 5 nm from $N = 3-7$ which is smaller than the error bars presented in the experiment by Haberland *et al.* From $N = 7$ there is virtually no blueshift. It is important to mention that our calculations are based on fitting the excitation energy for Ar_3^+ to 520 nm, therefore our spectra are expected to agree better with the spectra obtained by Levinger *et al.*, especially for small clusters. In summary, the evolution of the maximum peak as a function of the cluster size agrees very well with both experimental works. Although the qualitative results of the MBP model are similar to those without MBP for $N > 14$, it is clear that the inclusion of MBP is important for smaller clusters.

B. Hole delocalization using MBP

After each 10 Monte Carlo configurations the atoms are labeled in order of decreasing charge in the ground state. These configurations are saved for the calculation of the average charge for the different regions of the spectrum using the square of the transition dipole as a weighting factor. For all clusters, the average charge distribution in the ground state is localized in a trimer core. Figures 3 and 4 show the average charge in the excited states for different regions of the spectrum as a function of the nth atom ($1 \leqslant n \leqslant N$). Figures 3(a) and 3(b) show the excited state charge distribution for the ultraviolet (UV) region around 260 nm and the region around 425 nm for $N = 4$, 14, and 20. All cluster sizes follow the same trend, i.e., the hole is still localized in a trimer core. This is expected, since these two regions are already present in the photoabsorption spectrum for Ar_3^+. Figure 3(c) shows

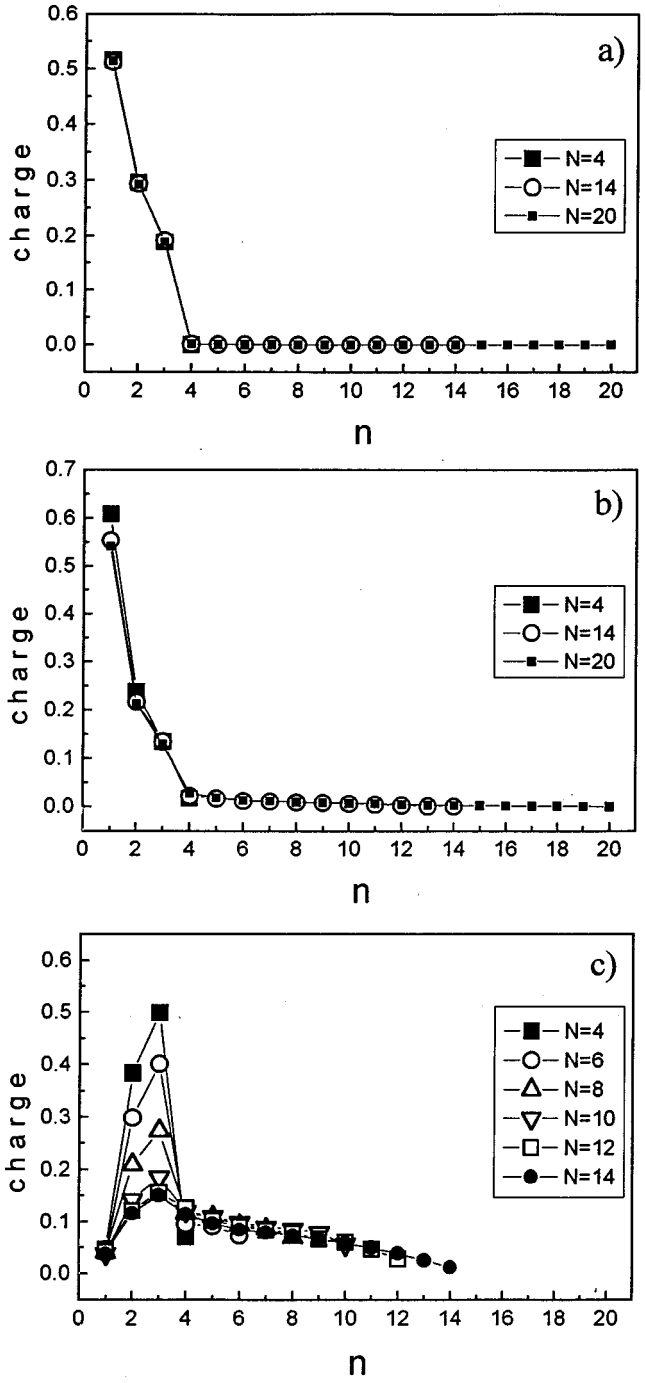

FIG. 3. Average hole distribution of the excited states as a function of the nth atom ($n \leqslant N$) for different regions of the spectrum. Atoms are labeled according to decreasing charge in the ground state. Representative cluster sizes are displayed. (a) UV region. (b) Region around 425 nm. (c) Main peak region around 520 nm for some cluster sizes with $N < 15$.

Downloaded 26 Apr 2004 to 130.132.248.10. Redistribution subject to AIP license or copyright, see http://jcp.aip.org/jcp/copyright.jsp

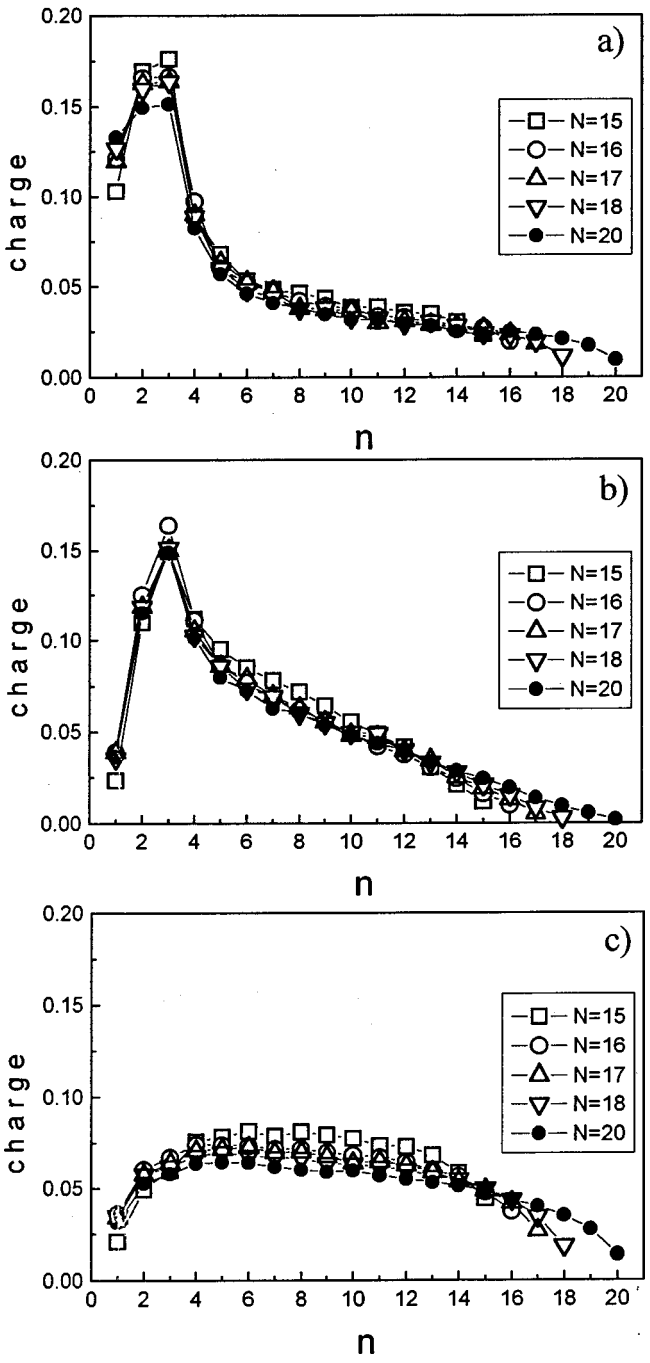

FIG. 4. Average hole distribution of the excited states as a function of the nth atom ($n \leqslant N$) for the low and high energy regions of the main peak. Representative cluster sizes with $N>15$ are displayed. (a) High energy region (from 470 to 515 nm). (b) Low energy region (from 515 to 650 nm). (c) Average hole distribution (from 470 to 615 nm) for states whose oscillator strengths are less than a cutoff [$|\boldsymbol{\mu}_{0a}(l)|^2 < 0.5(\text{a.u.})^2$].

the excited state charge distribution for the main peak around 520 nm for $N \leqslant 14$. A common feature for these cluster sizes is the almost zero charge on the first atom (central atom). As N increases, the hole is smoothly delocalized over the solvating atoms (atoms labeled $4-N$) accompanied by a decrease in charge on the core. This delocalization effect is correlated to the decreasing of the oscillator strength at the maximum of the peak and a consequent broadening of the photoabsorption spectrum. In our analysis of the main peak, we find

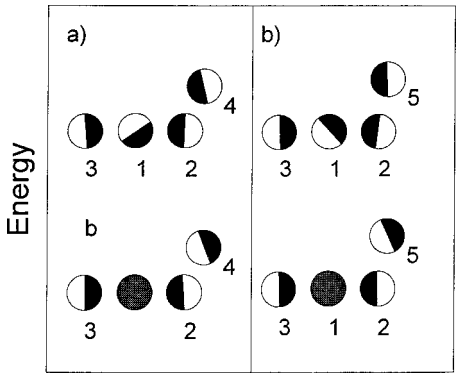

FIG. 5. Average geometry of the trimer core for $N=19$ with (a) the fourth solvating atom and (b) the fifth solvating atom. The average nodal structure is also shown.

contributions from three types of excited states. Two contributions are obvious for $N>14$ and lead to the low and high energy peaks that become resolved by $N=21$. A third contribution to the main peak comes from a large number of excited states with small transition moments; we refer to these states as the background.

To analyze the low and high energy regions of the main peak for $N>14$ we only use those excited states whose values of the transition dipole are larger than a certain cutoff. We choose the cutoff such that states with $|\boldsymbol{\mu}_{0a}(l)|^2 < 0.5(\text{a.u.})^2$ are classified as the background. The cutoff value is chosen to resolve the low and high energy peaks and therefore to estimate the wavelength interval for each region. The intervals are 470 and 515 nm for the high energy peak and 515 and 650 nm for the low energy peak. Figures 4(a) and 4(b) show the average charge for the high/low energy regions, respectively. In the high energy region, about 60% of the charge is localized in the first five atoms, consistent with a higher kinetic energy for that relatively high localization. In the low energy region, the charge is a little more delocalized (50% over the first five atoms), consistent with a lower kinetic energy. For the background, the charge is completely delocalized over the entire cluster [Fig. 4(c)].

Since the trimer core and the next two solvating atoms are the carriers of at least 50% of the charge, we investigate the average location of atoms 4 and 5 relative to the ion core and the average nodal structure of the electronic states. For the analysis of atom 4, each saved configuration is translated and rotated so that atom 1 is at the origin and atom 2 is on the positive $\hat{x}$ axis. The cluster is then rotated about the $\hat{x}$ axis so that atom 4 lies in the $\hat{x}\hat{y}$ plane with its $\hat{y}$ coordinate greater than zero. Two types of configurations arise, one with atom 4 near atom 2 (70% of the configurations) and the other with atom 4 near atom 3. A similar analysis was applied to the location of atom 5. We do not attempt to determine the correlations between the locations of atoms 4 and 5. Figure 5(a) shows the average geometry of the trimer core and the fourth solvating atom in its most probable position for the cluster with $N=19$. This is a representative cluster size where low and high energy regions are distinguished from the main peak. Two geometries are shown corresponding to the high and low energy regions. The average orientation of

Downloaded 26 Apr 2004 to 130.132.248.10. Redistribution subject to AIP license or copyright, see http://jcp.aip.org/jcp/copyright.jsp

the charge-carrying orbital on each atom is calculated by averaging the contributions from the three p orbitals on each atom and is indicated in Fig. 5. In the low energy region, atom 1 has almost no charge and the orbital on atom 4 overlaps constructively with the orbital on atom 2. In the high energy region atom 1 has about 13% of the charge and the orbital on atom 4 overlaps destructively with the orbital on atom 2, consistent with a higher energy. Figure 5(b) shows the average geometry for atom 5. In both the low and high energy regions the overlap between atom 5 and atom 2 seems to be constructive, although in the low energy region the overlap is more a σ bond while in the high energy region is more a π bond. In the high energy state, the orientation of atom 5 also appears to be correlated to the orientation of atom 1.

C. Energy optimization and magic numbers using MBP

We calculate the minimum energy geometry for the model with MBP by using the Powell minimization procedure[29] over the saved configurations during the MC run for $N<23$. The inclusion of MBP requires an $N\times N$ diagonalization for each diagonal term of the Hamiltonian, thus using conjugate gradient minimization (which requires the calculation of the gradient) would be practically impossible. Even using the Powell method the time needed to achieve the optimized geometry is considerable. Therefore, for $N=20-27$ we apply the Powell minimization to a single geometry which is obtained by conjugate gradient minimization over saved configurations using the model without MBP. This is justified as the optimized geometries with and without MBP are the same than those obtained[14,23] in DIM calculations for the range of sizes $N=20-27$.

There is no precise agreement among experiments,[11,12,30] or between experiments and calculations[14,21,23] in the assignment of magic numbers. In addition, there have been different ways to describe the stability of a cluster in the literature. Doltsinis *et al.*[23] reported $\Delta E_N=E_{N-1}-E_N$ and $\Delta_2 E=E_{N+1}+E_{N-1}-2E_N$ as a function of cluster size while Ikegami *et al.*[14] reported the relative binding energy $\Delta E_N/\Delta E_{N+1}$ as a measure of the cluster stability. Magic numbers are somewhat dependent upon which definition is used. We find magic numbers at $N=13$, 17, 19, 23, and 25 using $\Delta_2 E$ and $\Delta E_N/\Delta E_{N+1}$ and at $N=13$, 17, 19, 22, and 25 using ΔE_N (Fig. 6). Doltsinis *et al.* found a similar ambiguity under these definitions at $N=22$ and 23, although they found a magic number at $N=16$ rather than 17. Interestingly, Ikegami *et al.*[14] found magic numbers at $N=13$, 16, 19, 22, and 25 for all three definitions.

V. CONCLUSIONS

We presented a novel method in including many-body polarization interactions in the Hamiltonian model for Ar_N^+ ($N=3-23$). By comparing with experimental photoabsorption spectra we found very good agreement and noticed that inclusion of MBP is important for small clusters. We distinguished three components in the main peak of the spectra. In two of them, the low and high energy regions, the average

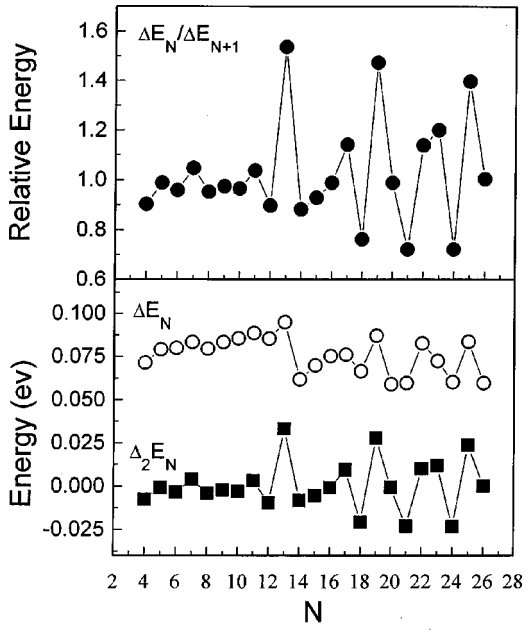

FIG. 6. (●) Relative binding energy as a function of cluster size. (○) First energy difference. (■) Second energy difference.

charge for the excited states at 80 K is mainly localized on five atoms. These atoms are the trimer core and two solvating atoms. These are the carriers of greater than 50% of the total charge. In the third region, the background, the charge is completely delocalized over the entire cluster. We used the Powell method to calculate the optimized geometries at 0 K and found the most stable clusters to be at $N=13$, 17, 19, 23, and 25.

[1] K. Horaoka and T. Mori, J. Chem. Phys. **90**, 7143 (1989).
[2] T. Nagata and T. Kondow, J. Chem. Phys. **98**, 290 (1993).
[3] W. Kamke, J. de Vries, J. Krauss, E. Kaiser, B. Kamke, and I. V. Hertel, Z. Phys. D: At., Mol. Clusters **14**, 330 (1989).
[4] G. Ganteför, G. Bröker, E. Holub-Krappe, and A. Ding, J. Chem. Phys. **91**, 7972 (1989).
[5] E. Rühl, C. Heinzel, H. Baumgärtel, M. Lavolléea, and P. Morin, Z. Phys. D: At., Mol. Clusters **31**, 245 (1994).
[6] H. Haberland, T. Kolar, C. Ludewigt, A. Rischa, and M. Schmidt, Z. Phys. D: At., Mol. Clusters **20**, 33 (1991).
[7] P. M. Dehmer and J. L. Dehmer, J. Chem. Phys. **69**, 125 (1978).
[8] M. J. Deluca and M. A. Johnson, Chem. Phys. Lett. **162**, 445 (1989).
[9] H. Haberland, B. V. Issendorff, H. Kornmeier, W. Orlik, T. Kolar, C. Ludewigt, T. Reiners, and A. Risch, in *Physics and Chemistry of Finite Systems: From Clusters to Crystals*, edited by P. Jena (Kluwer Academic, Norwell, MA, 1992), Vol. II, p. 943.
[10] N. E. Levinger, D. Ray, M. L. Alexander, and W. C. Lineberger, J. Chem. Phys. **89**, 5654 (1988).
[11] I. A. Harris, R. S. Kidwell, and J. A. Northby, Phys. Rev. Lett. **53**, 2390 (1984).
[12] A. Ding and J. Hesslich, Chem. Phys. Lett. **94**, 54 (1983).
[13] T. Ikegami and S. Iwata, J. Chem. Phys. **105**, 10734 (1996).
[14] T. Ikegami, T. Kondow, and S. Iwata, J. Chem. Phys. **98**, 3038 (1993).
[15] T. Ikegami, T. Kondow, and S. Iwata, J. Chem. Phys. **99**, 3588 (1993).
[16] I. Last and T. F. George, J. Chem. Phys. **93**, 8925 (1990).
[17] A. Goldberg, I. Last, and T. F. George, J. Chem. Phys. **100**, 8277 (1994).
[18] F. A. Gianturco, G. Delgado-Barrio, S. Miret-Artés, and P. Villarreal, Z. Phys. D: At., Mol. Clusters **35**, 115 (1995).
[19] A. Bastida, N. Halberstadt, J. A. Beswick, F. X. Gadéa, U. Buck, R. Galonska, and C. Lausnstein, Chem. Phys. Lett. **249**, 1 (1996).
[20] M. T. Bowers, W. E. Palke, K. Robins, C. Roehl, and S. Walsh, Chem. Phys. Lett. **180**, 235 (1991).

Downloaded 26 Apr 2004 to 130.132.248.10. Redistribution subject to AIP license or copyright, see http://jcp.aip.org/jcp/copyright.jsp

[21] G. A. Morales, J. Faulkner, and R. W. Hall, J. Chem. Phys. **109**, 3418 (1998).
[22] M. Grigorov and F. Spiegelmann, Surf. Rev. Lett. **3**, 211 (1996).
[23] N. L. Doltsinis, P. J. Knowles, and F. Y. Naumkin, Mol. Phys. **96**, 749 (1999).
[24] N. L. Doltsinis and P. J. Knowles, Chem. Phys. Lett. **301**, 241 (1999).
[25] H. Margenau and N. R. Kestner, *Theory of Intermolecular Forces*, 2nd ed. (Pergamon, Oxford, 1971).
[26] R. O. Watts and I. J. McGee, *Liquid State Chemical Physics* (Wiley, New York, 1976).
[27] J. Cao and B. J. Berne, J. Chem. Phys. **97**, 8628 (1992).
[28] W. R. Wadt, Appl. Phys. Lett. **38**, 1030 (1981).
[29] W. H. Press, B. P. Flannery, S. A. Teoukolsky, and W. T. Vetterling, *Numerical Recipies, The Art of Scientific Computing* (Cambridge University Press, Cambridge, 1986).
[30] S. Wei, Z. Shi, and A. W. Castleman, Jr., J. Chem. Phys. **94**, 8604 (1991).

Downloaded 26 Apr 2004 to 130.132.248.10. Redistribution subject to AIP license or copyright, see http://jcp.aip.org/jcp/copyright.jsp